Supplemental Information

Column XCO_2 Profile Analysis Further Details

Expanding on Eq. 1, the C parameter is equal to 2, representing an assumption that atmospheric carbon concentration has a linear gain from entrance to exit of the region due to the surface carbon flux. The wind velocity, V, is determined from MERRA2 lower tropospheric layer wind velocities (between 700 and 1000mb) (GMAO, 2015). L, or the effective path length of air flow through the region, is computed as the square root of the region area, or approximately 2150km in this case. M_{exp} is the ratio of the region's surface pressure to standard atmospheric pressure, for which surface pressure from MERRA2 was used. M is a factor that converts the mixing ratio concentration of carbon dioxide to mass including a conversion from CO_2 to C (or approximately 4.2×10^{-6} TgC/(km^2 ppmCO_2)). The mass balance method therefore models the increase of XCO_2 as air originating from the Pacific Ocean moves through a region with a surface carbon source. It partly requires knowing the wind speed and target region size to determine the residence time of air moving through the region.

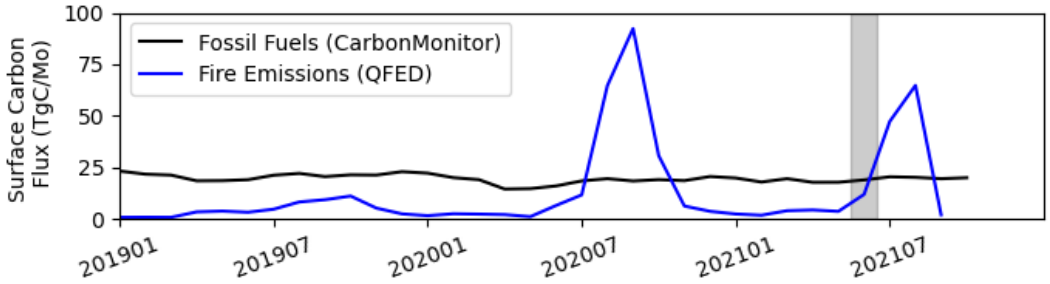

Fig. S1. Surface fossil fuel emissions based on CarbonMonitor. QFED fire emissions are shown for comparison as in Fig. 2C.

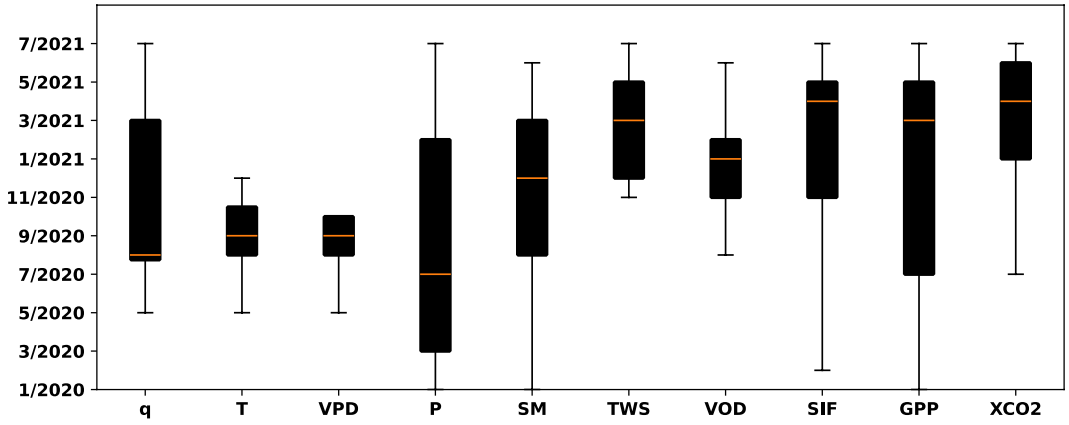

Fig. S2. Initial timing of the month when the soil-plant-atmosphere variables first became anomalous (|z-score|>1) between January 2020 and July 2021 (see methods). Same as the vertical line timing on Fig. 5. The boxplots are the distribution of the maximum anomaly timing for each pixel within the study region for each variable. q is AIRS boundary layer specific humidity, T is AIRS boundary layer air temperature, VPD is AIRS boundary layer vapor pressure deficit, P is GPM precipitation, SM is SMAP soil moisture, TWS is GRACE terrestrial water storage, VOD is SMAP vegetation optical depth, SIF is OCO-2 solar induced fluorescence, GPP is FluxSat gross primary production, and XCO_2 is OCO-2 column CO_2 atmospheric concentration.

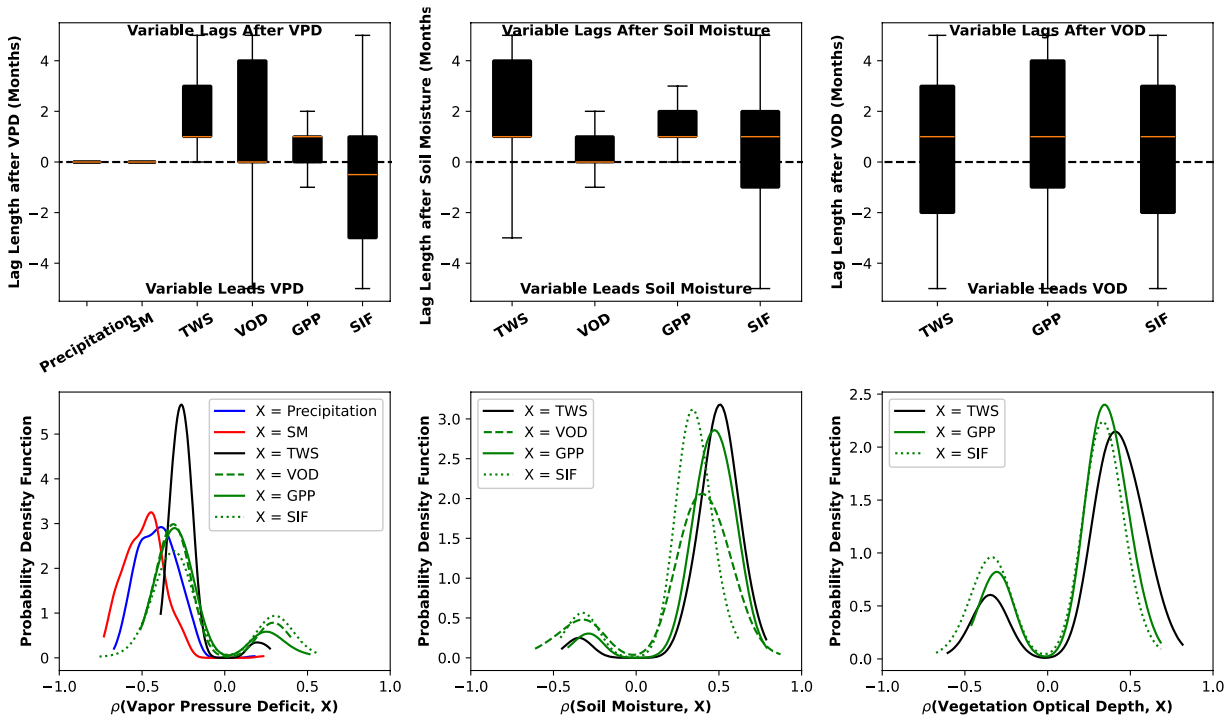

Fig. S3. Cross correlation analysis on a per pixel basis. Top row: Lags at maximum absolute correlation of monthly anomalies. Bottom row: maximum lagged correlation value. Both plots show spatial distributions of values in the Western US.

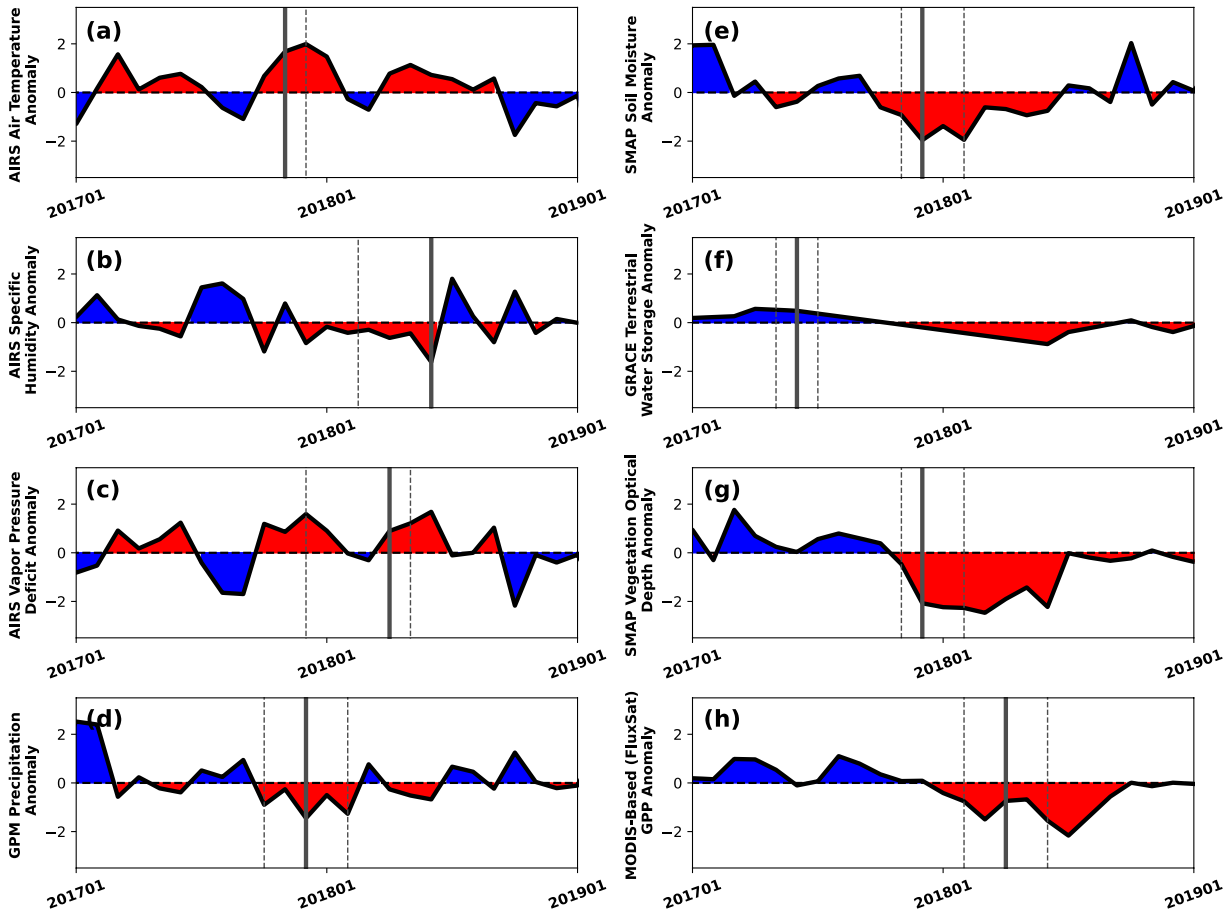

Fig. S4. Same as Figure 5, but for the Southwest US during a dry cascade in 2018 (latitude: 33ºN-41ºN, longitude: 125ºW-104ºW). Note that GRACE TWS was unavailable from late 2017 through 2018.

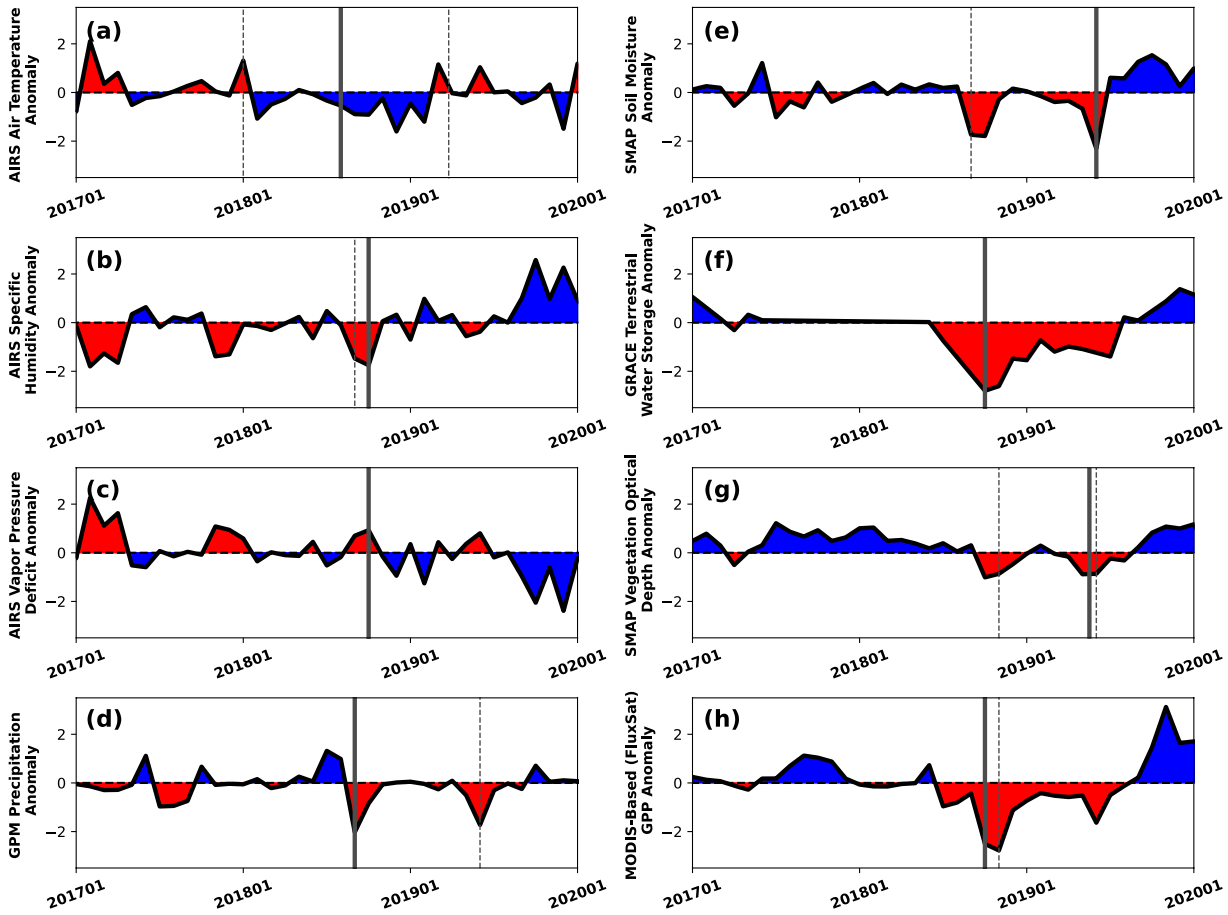

Fig. S5. Same as Figure 5, but for a dry cascade in India in 2018 (latitude: 16ºN-21ºN, longitude: 75ºE-80ºE). Note that GRACE TWS was unavailable from late 2017 through 2018.

Further Details on the Granger Causality Casual Linear Model

Eq. 2 is carried out similarly to previous GC applications (Green et al., 2017; Mosedale et al., 2006; Tuttle and Salvucci, 2016). This equation is performed on the January 2003 to December 2019 monthly anomalies of these variables. The inherent monthly timescale of TWS prevented assessing this equation at shorter timescales. Furthermore, error correlations between the variables are likely negligible because they originate from different observation sources. FluxSat GPP is also driven only by MODIS reflectivity measurements and FLUXNET observations and is not driven by forcing from environmental variables. p lags are optimized using quasi-information criterion (QIC), which provides results intermediary between commonly used AIC and BIC. Optimal lags were chosen between 1, 2, and 3 months with typically high QIC beyond 3 months.

Significance in Eq. 3 is additionally tested for the common regression assumption violation of autocorrelated errors using the Newey-West covariance matrix of the regression coefficients (Newey and West, 1987). We found a general increase in p-values due to autocorrelation, but this did not change the spatial pattern of detected GC connection of TWS to GPP.

It is well-known that environmental variable interactions with plants tend to be linear in water-limited locations in the water-limited evaporative regime (Feldman et al., 2020; Short Gianotti et al., 2019). Therefore, we anticipate that the linear model is generally sufficient to describe the GPP linear response to climate in the Western US.

Further Details on Statistical Detection of GPP Resilience and Amplification Effects

After detection of causal influences, we perform two tests with this linear model to detect whether GRACE TWS offered GPP resilience in 2020 and detect whether influences other than the environment drove the large GPP deficit in 2021 (i.e., legacy effects related to plant physiological factors). We perform these tests only in pixels where TWS causal influence on GPP is detected. At the expense of not explaining the response of the entire region, this choice provides robustness in physical interpretation for both tests. Therefore, these tests will not quantify the respective phenomena's effects on the overall Western US response and carbon budget, but are used as a robust detection of the given phenomenon. For the resilience test, the established statistical connection between TWS and GPP is required to establish a Granger-causal influence of TWS to reduce GPP deficits. This constraint also sets a conservative bound on the legacy test because regions where TWS influences GPP tend to have larger TWS deficits (Fig. S7). Therefore, these pixels are expected to come closest to being able to model the large GPP deficit, given a larger TWS deficit and causal connection between TWS and GPP.

To test for GPP resilience in 2020, we first use the full, unrestricted model (Eq. 2) to predict the spatially averaged FluxSat GPP signal. This modeled series, named the "Causal Model Baseline," serves as a baseline for comparison against subsequent tests. For "Resilience Test 1," we then set the 2020 TWS time steps to the mean TWS anomaly between January and July 2021 and repeat Eq. 2. For "Resilience Test 2," we repeat Resilience Test 1, but remove the autoregressive GPP term in Eq. 2 to isolate the linear effects of the environment (rainfall, VPD, TWS) on GPP more closely. More negative GPP anomalies produced by the resilience tests than that of the baseline suggest that TWS offered GPP resilience in 2020. The GPP autoregressive component tends to explain most of the GPP variability and may cause underestimates of the effects of TWS on GPP. Therefore, Resilience Tests 1 and 2 serve as lower and upper bounds of the degree of resilience, respectively.

Finally, deviations in model performance can indicate the inability to explain GPP variations in 2020 and 2021 that are due to non-linear interactions with climate or biophysical factors. We test for nonlinear effects by fitting Eq. 2 with ("Extreme Amplification Test 1") and without ("Extreme Amplification Test 2") the autoregressive GPP component. Amplification effects are expected to be detected when the tests predict less negative GPP anomalies in 2021 than that in the FluxSAT GPP time series. Extreme Amplification Test 1 serves as a conservative test: the added effects performing the test in regions of TWS GC-causal influence on GPP, having TWS have more negative anomalies in these regions, and accounting for GPP persistence and compounding effects should all produce the most negative GPP anomalies. Extreme Amplification Test 2 further isolates linear interactions of climate on GPP and partitions out any GPP persistence as observed in the available time series.

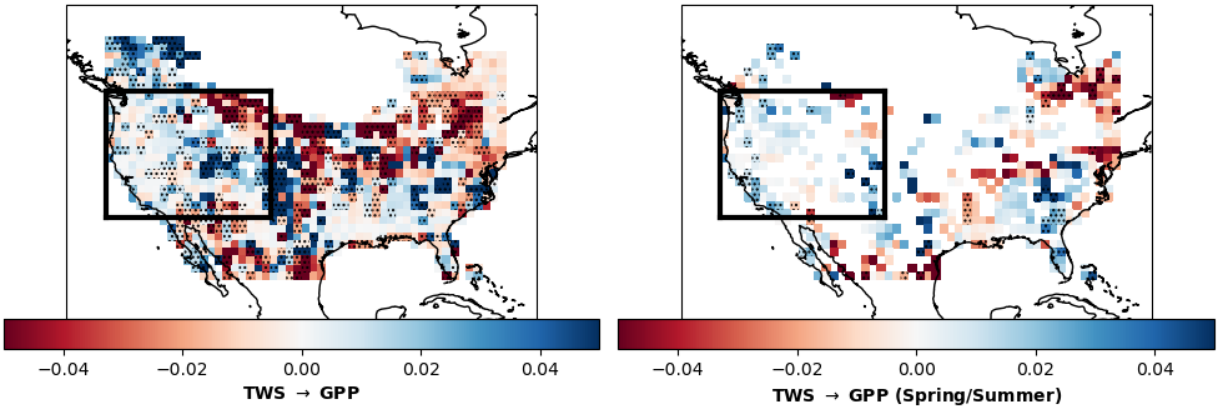

Fig. S6. Same as Fig. 7A, but using SMAP soil moisture between April 2015 and December 2020. TWS Granger-causes GPP in 31% of the study region over the full time series. This decreases to 20% for spring and summer months, but only 41% of the study region had enough data to do the Granger causality analysis in these months. Data were extended to 2020 to increase sample size. Pixels with no values have less than 20 months of data largely preventing the Granger causality analysis.

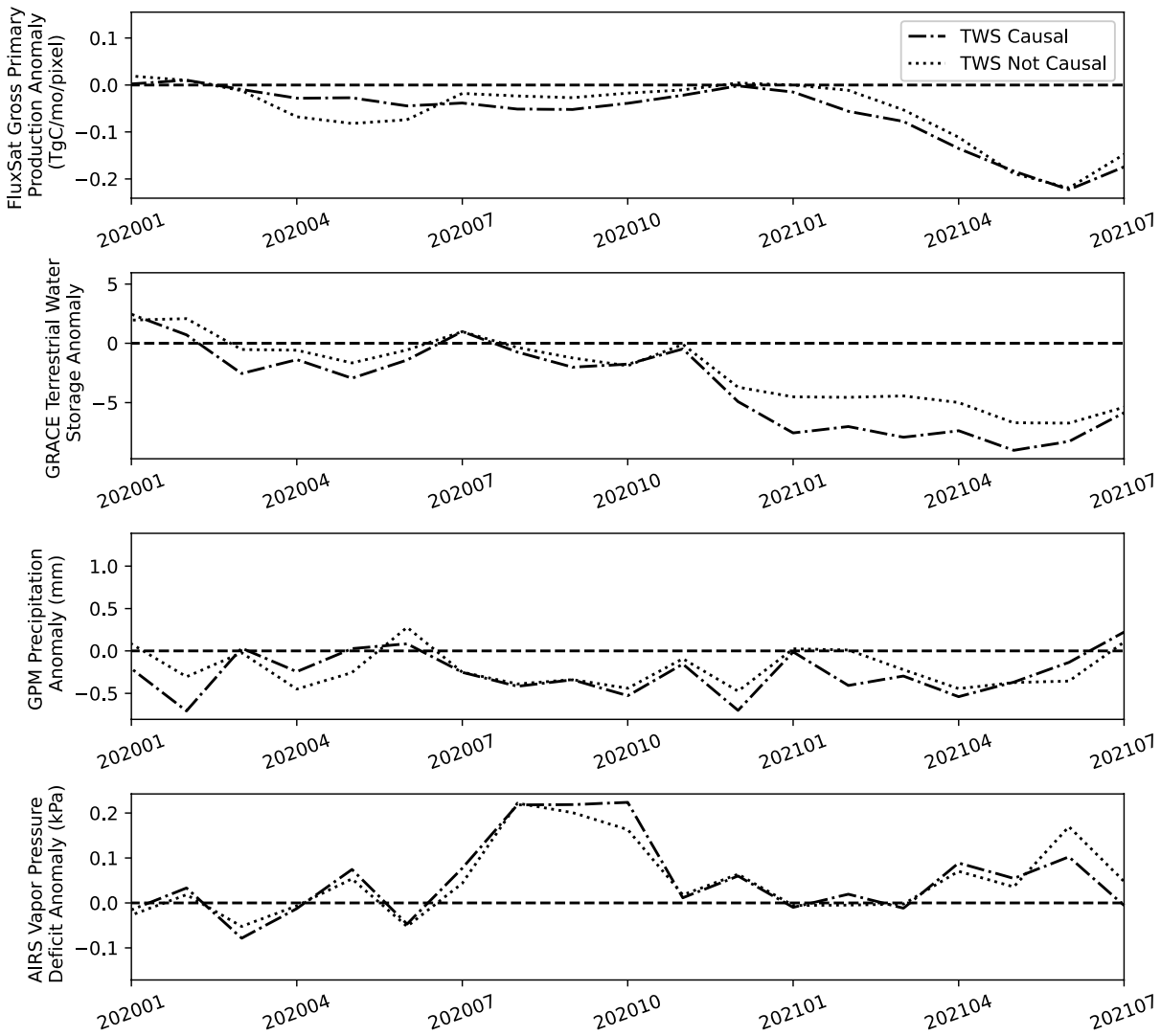

Fig. S7. Observed differences in FluxSat gross primary production (GPP), GRACE terrestrial water storage (TWS), GPM precipitation (P), and AIRS vapor pressure deficit (VPD) between pixels where TWS Granger-causes GPP ("TWS Causal") and where it does not ("TWS Not Causal"). Pixels with non-causal or causal TWS influence were averaged to create the time series.

References

Bastos, A., Orth, R., Reichstein, M., Ciais, P., Viovy, N., Zaehle, S., Anthoni, P., Arneth, A., Gentine, P., Joetzjer, E., Lienert, S., Loughran, T., McGuire, P.C., Sungmin, O., Pongratz, J., Sitch, S., 2021. Vulnerability of European ecosystems to two compound dry and hot summers in 2018 and 2019. Earth Syst. Dyn. 12, 1015–1035. https://doi.org/10.5194/esd-12-1015-2021

Buchwitz, M., Reuter, M., Noël, S., Bramstedt, K., Schneising, O., Hilker, M., Fuentes Andrade, B., Bovensmann, H., Burrows, J.P., Di Noia, A., Boesch, H., Wu, L., Landgraf, J., Aben, I., Retscher, C., O'Dell, C.W., Crisp, D., 2021. Can a regional-scale reduction of atmospheric CO2during the COVID-19 pandemic be detected from space? A case study for East China using satellite XCO2retrievals. Atmos. Meas. Tech. 14, 2141–2166. https://doi.org/10.5194/amt-14-2141-2021

Buchwitz, M., Schneising, O., Reuter, M., Heymann, J., Krautwurst, S., Bovensmann, H., Burrows, J.P., Boesch, H., Parker, R.J., Somkuti, P., Detmers, R.G., Hasekamp, O.P., Aben, I., Butz, A., Frankenberg, C., Turner, A.J., 2017. Satellite-derived methane hotspot emission estimates using a fast data-driven method. Atmos. Chem. Phys. 17, 5751–5774. https://doi.org/10.5194/acp-17-5751-2017

Feldman, A.F., Short Gianotti, D.J., Trigo, I.F., Salvucci, G.D., Entekhabi, D., 2020. Land-atmosphere drivers of landscape-scale plant water content loss. Geophys. Res. Lett. 47, e2020GL090331.

GMAO, 2015. MERRA-2 inst1_2d_asm_Nx: 2d,1-Hourly,Instantaneous,Single-Level,Assimilation,Single-Level Diagnostics V5.12.4, Greenbelt, MD, USA, Goddard Earth Sciences Data and Information Services Center (GES DISC), Accessed: [01.10.19], 10.5067/3Z173KIE2TPD.

Granger, C.W.J., 1969. Investigating Causal Relations by Econometric Models and Cross-spectral Methods. Econometrica 37, 424–438.

Green, J.K., Konings, A.G., Alemohammad, S.H., Berry, J., Entekhabi, D., Kolassa, J., Lee, J.E., Gentine, P., 2017. Regionally strong feedbacks between the atmosphere and terrestrial biosphere. Nat. Geosci. 10, 410–414. https://doi.org/10.1038/ngeo2957

Greene, W.H., 2003. Econometric Analysis. Prentice Hall, New York.

Mckee, T.B., Doesken, N.J., Kleist, J., 1993. The relationship of drought frequency and duration to time scales. AMS 8th Conf. Appl. Climatol. 179–184. https://doi.org/citeulike-article-id:10490403

Mosedale, T.J., Stephenson, D.B., Collins, M., Mills, T.C., 2006. Granger causality of coupled climate processes: Ocean feedback on the North Atlantic Oscillation. J. Clim. 19, 1182–1194. https://doi.org/10.1175/JCLI3653.1

Newey, W.K., West, K.D., 1987. A Simple, Positive Semi-definite, Heteroskedasticity and Autocorrelation Consistent Covariance Matrix. Econometrica 55, 703–708.

Peters, W., Jacobson, A.R., Sweeney, C., Andrews, A.E., Conway, T.J., Masarie, K., Miller, J.B., Bruhwiler, L.M.P., Pétron, G., Hirsch, A.I., Worthy, D.E.J., Van Der Werf, G.R., Randerson, J.T., Wennberg, P.O., Krol, M.C., Tans, P.P., 2007. An atmospheric perspective on North American carbon dioxide exchange: CarbonTracker. Proc. Natl. Acad. Sci. U. S. A. 104, 18925–18930. https://doi.org/10.1073/pnas.0708986104

Short Gianotti, D.J., Rigden, A.J., Salvucci, G.D., Entekhabi, D., 2019. Satellite and Station Observations Demonstrate Water Availability's Effect on Continental-Scale Evaporative and Photosynthetic Land Surface Dynamics. Water Resour. Res.

https://doi.org/10.1029/2018WR023726
Stocker, B.D., Zscheischler, J., Keenan, T.F., Prentice, I.C., Seneviratne, S.I., Peñuelas, J., 2019. Drought impacts on terrestrial primary production underestimated by satellite monitoring. Nat. Geosci. 12, 264–270. https://doi.org/10.1038/s41561-019-0318-6
Tuttle, S., Salvucci, G., 2016. Empirical evidence of contrasting soil moisutre-precipitation feedbacks across the United States. Science (80-.). 352, 825–827.
Tuttle, S.E., Salvucci, G.D., 2017. Confounding factors in determining causal soil moisture-precipitation feedback. Water Resour. Res. 5531–5544. https://doi.org/10.1002/2016WR019869